REPORT DOCUMENTATION PAGE

Form Approved
OMB No. 0704-0188

1. REPORT DATE *(DD-MM-YYYY)*	2. REPORT TYPE	3. DATES COVERED *(From - To)*
06/01/2014	Technical Report - Final Report	

4. TITLE AND SUBTITLE
Isogeometric Phase-field Simulation of Boiling

5a. CONTRACT NUMBER

5b. GRANT NUMBER

5c. PROGRAM ELEMENT NUMBER

6. AUTHOR(S)

5d. PROJECT NUMBER

5e. TASK NUMBER

5f. WORK UNIT NUMBER

7. PERFORMING ORGANIZATION NAME(S) AND ADDRESS(ES)
University of Texas at Austin Austin TX United States

8. PERFORMING ORGANIZATION REPORT NUMBER

9. SPONSORING/MONITORING AGENCY NAME(S) AND ADDRESS(ES)
Office of Naval Research Arlington VA United States

10. SPONSOR/MONITOR'S ACRONYM(S)

11. SPONSOR/MONITOR'S REPORT NUMBER(S)

12. DISTRIBUTION/AVAILABILITY STATEMENT
A = Approved For Public Release 12/2/2015 No

13. SUPPLEMENTARY NOTES

14. ABSTRACT
In this work we consider the Navier-Stokes-Korteweg equations, a diffuseinterface model describing liquid-vapor phase transitions. A numerical scheme for this model is constructed based on functional entropy variables and a new time integration concept. The fully discrete scheme is unconditionally stable in entropy and second-order time-accurate. Isogeometric analysis is utilized for spatial discretization. The boiling problem is numerically investigated by making proper assumptions

15. SUBJECT TERMS

16. SECURITY CLASSIFICATION OF:			17. LIMITATION OF ABSTRACT	18. NUMBER OF PAGES	19a. NAME OF RESPONSIBLE PERSON
a. REPORT	b. ABSTRACT	c. THIS PAGE			19b. TELEPHONE NUMBER *(Include area code)*
U	U	U			

ICES REPORT 15-16

June 2015

Isogeometric Phase-field Simulation of Boiling

by

Ju Liu, Thomas J.R. Hughes

The Institute for Computational Engineering and Sciences
The University of Texas at Austin
Austin, Texas 78712

Reference: Ju Liu, Thomas J.R. Hughes, "Isogeometric Phase-field Simulation of Boiling ," ICES REPORT 15-16, The Institute for Computational Engineering and Sciences, The University of Texas at Austin, June 2015.

Isogeometric Phase-field Simulation of Boiling

Ju Liu and Thomas J.R. Hughes

This paper is dedicated to Tayfun E. Tezduyar on the occasion of his 60th birthday.

Abstract In this work we consider the Navier-Stokes-Korteweg equations, a diffuse-interface model describing liquid-vapor phase transitions. A numerical scheme for this model is constructed based on functional entropy variables and a new time integration concept. The fully discrete scheme is unconditionally stable in entropy and second-order time-accurate. Isogeometric analysis is utilized for spatial discretization. The boiling problem is numerically investigated by making proper assumptions on transport parameters and boundary conditions. Compared with traditional multiphase solvers, the dependence on empirical data is significantly reduced, and this modeling approach provides a unified predictive tool for both nucleate and film boiling. Both two- and three-dimensional simulation results are provided.

1 Introduction

Boiling is a thermally induced phase transition process in which new liquid-vapor interfaces are generated in a bulk liquid region [2]. It is an extremely effective mechanism in energy transfer and is widely used in energy conversion facilities. Despite its importance in industry, the fundamental mechanism of boiling is still not well understood [2]. A predictive model for boiling is highly desired for engineering designs. Film boiling is regarded as most amenable to modeling, since its governing mechanism is principally the Rayleigh-Taylor instability. However, existing simulations all start with a preexisting perturbed flat interface as the initial condition [8]. In other words, none of those methods captured the film generation process. On the

Ju Liu
Institute for Computational Engineering and Sciences, The University of Texas at Austin, 201 East 24th Street, 1 University Station C0200, Austin, TX 78712, USA e-mail: jliu@ices.utexas.edu

Thomas J.R. Hughes
Institute for Computational Engineering and Sciences, The University of Texas at Austin, 201 East 24th Street, 1 University Station C0200, Austin, TX 78712, USA e-mail: hughes@ices.utexas.edu

other side, very few simulations of nucleate boiling have been performed because more physical mechanisms are involved in this phenomenon.

Traditional interface-tracking and interface-capturing methods are designed based on geometrical information of existing interfaces. This is perhaps the reason why these methods become intractable for phase transition phenomena. Phase-field or diffuse-interface methods were proposed as an alternative interface-capturing method, that use thermodynamic state variables to distinguish different phases [1]. The solid mathematical and thermodynamic foundations of phase-field models allow them to describe these complicated phenomena without resorting to modeling "tricks." The initial instantiation of phase-field methods is the Navier-Stokes-Korteweg equations, which are constructed based on the van der Waals theory [1, 4]. In the past decades, this theory has been developed further [3], and a rational thermomechanical framework for the Navier-Stokes-Korteweg equations has been presented very recently [10].

For phase-field problems, the non-convexity of the entropy function precludes the possibility of directly applying many existing robust numerical methodologies [11]. To overcome the challenges posed by the non-convexity of the entropy, first, functional entropy-variables are introduced to construct an entropy-stable spatial discretization [9, 10]. Second, to develop a stable temporal scheme, we adopt the methodology based on special quadrature rules [5, 9]. This time integration concept can be viewed as a second-order modification to the mid-point rule. The modifications are designed so that the temporal approximation is provably entropy dissipative. Since this temporal scheme does not require convexity for the entropy function, it is anticipated to be applicable to many more general problems.

2 The Navier-Stokes-Korteweg equations

We consider a fixed, connected, and bounded domain $\Omega \subset \mathbb{R}^3$. The time interval of interest is denoted $(0,T)$, with $T > 0$. The dimensionless Navier-Stokes-Korteweg equations are considered in the space-time domain $\Omega \times (0,T)$ as

$$\frac{\partial \rho}{\partial t} + \nabla \cdot (\rho \mathbf{u}) = 0, \tag{1}$$

$$\frac{\partial (\rho \mathbf{u})}{\partial t} + \nabla \cdot (\rho \mathbf{u} \otimes \mathbf{u}) + \nabla p - \nabla \cdot \boldsymbol{\tau} - \nabla \cdot \boldsymbol{\varsigma} = \rho \mathbf{b}, \tag{2}$$

$$\frac{\partial (\rho E)}{\partial t} + \nabla \cdot ((\rho E + p)\mathbf{u} - (\boldsymbol{\tau} + \boldsymbol{\varsigma})\mathbf{u}) + \nabla \cdot \mathbf{q} + \nabla \cdot \boldsymbol{\Pi} = \rho \mathbf{b} \cdot \mathbf{u} + \rho r. \tag{3}$$

In the above equations, ρ is the density, $\mathbf{u}$ is the velocity, E is the total energy, p is the thermodynamic pressure, $\boldsymbol{\tau}$ is the viscous stress, $\boldsymbol{\varsigma}$ is the Korteweg stress, $\mathbf{q}$ is the heat flux; $\boldsymbol{\Pi}$ is the interstitial working flux [3, 10], $\mathbf{b}$ is the prescribed body force per unit mass, and r is the heat source per unit mass. The constitutive relations are

$$p = \frac{8\theta\rho}{27(1-\rho)} - \rho^2, \qquad \boldsymbol{\tau} = \frac{1}{\mathrm{Re}}\left(\nabla\mathbf{u} + \nabla\mathbf{u}^T - \frac{2}{3}\nabla\cdot\mathbf{u}\mathbf{I}\right), \qquad \mathbf{q} = -\kappa\nabla\theta,$$
$$\boldsymbol{\varsigma} = \frac{1}{\mathrm{We}}\left(\left(\rho\Delta\rho + \frac{1}{2}|\nabla\rho|^2\right)\mathbf{I} - \nabla\rho\otimes\nabla\rho\right), \qquad \iota_{loc} = -\rho + \frac{8}{27(\gamma-1)}\theta,$$
$$\iota = \iota_{loc} + \frac{1}{2\mathrm{We}\rho}|\nabla\rho|^2, \qquad E = \iota + \frac{1}{2}|\mathbf{u}|^2, \qquad \boldsymbol{\Pi} = \frac{1}{\mathrm{We}}\rho\nabla\cdot\mathbf{u}\nabla\rho,$$

wherein θ is the temperature, κ is the conductivity, Re is the Reynolds number, We is the Weber number, γ is the heat capacity ratio, and ι is the internal energy density per unit mass. The mathematical entropy function H and the local Helmholtz free energy Ψ_{loc} are defined as

$$H := \frac{8}{27}\rho\ln\left(\frac{\rho}{1-\rho}\right) - \frac{8}{27(1-\gamma)}\rho\ln(\theta),$$
$$\Psi_{loc}(\rho,\theta) := -\rho + \frac{8}{27(\gamma-1)}\theta + \frac{8}{27}\theta\ln\left(\frac{\rho}{1-\rho}\right) - \frac{8}{27(1-\gamma)}\theta\ln\theta.$$

In three dimensions, the vector of conservation variables is

$$\mathbf{U}^T = [U_1,U_2,U_3,U_4,U_5] := [\rho,\rho u_1,\rho u_2,\rho u_3,\rho E].$$

Due to the appearance of the gradient-squared term, the mathematical entropy function H is no longer just an algebraic function of the conservation variables, but rather it is a functional of the conservation variables. We define the entropy variables $\mathbf{V}^T = [V_1,V_2,V_3,V_4,V_5]$ as the functional derivatives of H with respect to $\mathbf{U}$:

$$V_i[\delta v_i] = \frac{\delta H}{\delta U_i}[\delta v_i], \quad i = 1,\ldots,5,$$

wherein $\delta\mathbf{v}^T = [\delta v_1,\delta v_2,\delta v_3,\delta v_4,\delta v_5]$ are the test functions. The entropy variables $\mathbf{V}$ can be written explicitly as

$$V_1[\delta v_1] = \frac{1}{\theta}\left(\nu_{loc} - \frac{|\mathbf{u}|^2}{2}\right)\delta v_1 + \frac{1}{\mathrm{We}}\frac{1}{\theta}\nabla\rho\cdot\nabla\delta v_1,$$
$$V_i[\delta v_i] = \frac{u_{i-1}}{\theta}\delta v_i, \quad i = 2,3,4, \quad V_5[\delta v_5] = -\frac{1}{\theta}\delta v_5,$$

wherein

$$\nu_{loc} = -2\rho + \frac{8}{27}\theta\ln\left(\frac{\rho}{1-\rho}\right) - \frac{8}{27(\gamma-1)}\theta(\ln(\theta)-1) + \frac{8\theta}{27(1-\rho)}$$

is the local electrochemical potential. Inspired from the form of V_1, we introduce a new independent variable V as

$$V := \frac{1}{\theta}\left(\nu_{loc} - \frac{|\mathbf{u}|^2}{2}\right) - \frac{1}{\mathrm{We}}\nabla\cdot\left(\frac{\nabla\rho}{\theta}\right).$$

The fundamental thermodynamic relation between p and ν_{loc} allows us to express p in terms of V as

$$p = \rho V\theta - \rho\Psi_{loc} + \frac{\rho|\mathbf{u}|^2}{2} + \frac{1}{\mathrm{We}}\rho\theta\nabla\cdot\left(\frac{\nabla\rho}{\theta}\right). \tag{4}$$

Making use of the relation (4), the original strong-form problem (1)-(3) can be rewritten as

$$\frac{\partial\rho}{\partial t} + \nabla\cdot(\rho\mathbf{u}) = 0, \tag{5}$$

$$\begin{aligned}&\frac{\partial(\rho\mathbf{u})}{\partial t} + \nabla\cdot(\rho\mathbf{u}\otimes\mathbf{u}) + \nabla\left(\rho V\theta + \frac{\rho|\mathbf{u}|^2}{2} + \frac{1}{\mathrm{We}}\rho\theta\nabla\cdot\left(\frac{\nabla\rho}{\theta}\right)\right)\\ &\quad - \left(V\theta + \frac{|\mathbf{u}|^2}{2} + \frac{1}{\mathrm{We}}\theta\nabla\cdot\left(\frac{\nabla\rho}{\theta}\right)\right)\nabla\rho - H\nabla\theta - \nabla\cdot\boldsymbol{\tau} - \nabla\cdot\boldsymbol{\varsigma} = \rho\mathbf{b},\end{aligned} \tag{6}$$

$$\begin{aligned}&\frac{\partial(\rho E)}{\partial t} + \nabla\cdot\left(\left(\rho V\theta - \theta H + \frac{1}{2\mathrm{We}}|\nabla\rho|^2 + \rho|\mathbf{u}|^2 + \frac{1}{\mathrm{We}}\rho\theta\nabla\cdot\left(\frac{\nabla\rho}{\theta}\right)\right)\mathbf{u}\right)\\ &\quad -\nabla\cdot((\boldsymbol{\tau}+\boldsymbol{\varsigma})\mathbf{u}) + \nabla\cdot\mathbf{q} + \nabla\cdot\boldsymbol{\Pi} = \rho\mathbf{b}\cdot\mathbf{u} + \rho r,\end{aligned} \tag{7}$$

$$V = \frac{1}{\theta}\left(\nu_{loc} - \frac{|\mathbf{u}|^2}{2}\right) - \frac{1}{\mathrm{We}}\nabla\cdot\left(\frac{\nabla\rho}{\theta}\right). \tag{8}$$

The new strong-form problem (5)-(8) is an equivalent statement of the original Navier-Stokes-Korteweg equations (1)-(3).

3 The fully discrete scheme

The time interval $(0,T)$ is divided into N_{ts} subintervals (t_n, t_{n+1}), $n = 0,\cdots,N_{ts}-1$, of size $\Delta t_n = t_{n+1} - t_n$. We use the notation

$$\boldsymbol{Y}_n^h := \left[\rho_n^h, \frac{u_{1,n}^h}{\theta_n^h}, \frac{u_{2,n}^h}{\theta_n^h}, \frac{u_{3,n}^h}{\theta_n^h}, \frac{-1}{\theta_n^h}, V_n^h\right]^T$$

to represent the fully discrete solutions at the time level n. We define the jump of density, linear momentum, and total energy over each time step as

$$\begin{aligned}[\![\rho_n^h]\!] &:= \rho_{n+1}^h - \rho_n^h, \quad [\![\rho_n^h\mathbf{u}_n^h]\!] := \rho_{n+1}^h\mathbf{u}_{n+1}^h - \rho_n^h\mathbf{u}_n^h,\\ \left[\rho_n^h E(\rho_n^h,\mathbf{u}_n^h,\theta_n^h)\right] &:= (\rho\Psi_{loc})(\rho_{n+\frac{1}{2}}^h,\theta_{n+1}^h) - (\rho\Psi_{loc})(\rho_{n+\frac{1}{2}}^h,\theta_n^h)\\ &\quad +(\rho\Psi_{loc})(\rho_{n+1}^h,\theta_{n+\frac{1}{2}}^h) - (\rho\Psi_{loc})(\rho_n^h,\theta_{n+\frac{1}{2}}^h)\\ &\quad -\theta_{n+\frac{1}{2}}^h\left(H(\rho_{n+1}^h,\theta_{n+1}^h) - H(\rho_n^h,\theta_n^h)\right)\end{aligned}$$

$$
\begin{aligned}
&-\frac{\theta^h_{n+1}-\theta^h_n}{2}\left(H(\rho^h_{n+\frac{1}{2}},\theta^h_{n+1})+H(\rho^h_{n+\frac{1}{2}},\theta^h_n)\right)\\
&+\frac{(\theta^h_{n+1}-\theta^h_n)^3}{12}\frac{\partial^2 H}{\partial\theta^2}(\rho^h_{n+\frac{1}{2}},\theta^h_{n+1})\\
&+\frac{1}{2}\left(\rho^h_{n+1}|\mathbf{u}^h_{n+1}|^2-\rho^h_n|\mathbf{u}^h_n|^2\right)+\frac{1}{2\mathrm{We}}\left(|\nabla\rho^h_{n+1}|^2-|\nabla\rho^h_n|^2\right).
\end{aligned}
$$

With the jump operators defined above, the fully discrete scheme can be stated as follows. In each time step, given $\mathbf{Y}^h_n$ and the time step Δt_n, find $\mathbf{Y}^h_{n+1}$ such that for all $w^h_1\in\mathscr{V}^h$, $\mathbf{w}^h=(w^h_2;w^h_3;w^h_4)^T\in\left(\mathscr{V}^h\right)^3$, $w^h_5\in\mathscr{V}^h$, and $w^h_6\in\mathscr{V}^h$,

$$
\mathbf{B}^M(w^h_1;\mathbf{Y}^h_{n+1}):=\left(w^h_1,\frac{[\![\rho^h_n]\!]}{\Delta t_n}\right)_\Omega-\left(\nabla w^h_1,\rho^h_{n+\frac{1}{2}}\mathbf{u}^h_{n+\frac{1}{2}}\right)_\Omega=0, \tag{9}
$$

$$
\begin{aligned}
\mathbf{B}^U(\mathbf{w}^h;\mathbf{Y}^h_{n+1}):=&\left(\mathbf{w}^h,\frac{[\![\rho^h_n\mathbf{u}^h_n]\!]}{\Delta t_n}\right)_\Omega-\left(\nabla\mathbf{w}^h,\rho^h_{n+\frac{1}{2}}\mathbf{u}^h_{n+\frac{1}{2}}\otimes\mathbf{u}^h_{n+\frac{1}{2}}\right)_\Omega\\
&-\left(\nabla\cdot\mathbf{w}^h,\rho^h_{n+\frac{1}{2}}V^h_{n+\frac{1}{2}}\theta^h_{n+\frac{1}{2}}+\frac{1}{2}\rho^h_{n+\frac{1}{2}}|\mathbf{u}^h_{n+\frac{1}{2}}|^2+\frac{1}{\mathrm{We}}\rho^h_{n+\frac{1}{2}}\theta^h_{n+\frac{1}{2}}\nabla\cdot\left(\frac{\nabla\rho^h_{n+\frac{1}{2}}}{\theta^h_{n+\frac{1}{2}}}\right)\right)_\Omega\\
&-\left(\mathbf{w}^h,\left(V^h_{n+\frac{1}{2}}\theta^h_{n+\frac{1}{2}}+\frac{|\mathbf{u}^h_{n+\frac{1}{2}}|^2}{2}+\frac{1}{\mathrm{We}}\theta^h_{n+\frac{1}{2}}\nabla\cdot\left(\frac{\nabla\rho^h_{n+\frac{1}{2}}}{\theta^h_{n+\frac{1}{2}}}\right)\right)\nabla\rho^h_{n+\frac{1}{2}}\right)_\Omega\\
&-\left(\mathbf{w}^h,H^h_{n+\frac{1}{2}}\nabla\theta^h_{n+\frac{1}{2}}\right)_\Omega+\left(\nabla\mathbf{w}^h,\boldsymbol{\tau}^h_{n+\frac{1}{2}}+\boldsymbol{\varsigma}^h_{n+\frac{1}{2}}\right)_\Omega-\left(\mathbf{w}^h,\rho^h_{n+\frac{1}{2}}\mathbf{b}\right)_\Omega=\mathbf{0},
\end{aligned} \tag{10}
$$

$$
\begin{aligned}
\mathbf{B}^E(w^h_5;\mathbf{Y}^h_{n+1}):=&\left(w^h_5,\frac{\left[\rho^h_nE(\rho^h_n,\mathbf{u}^h_n,\theta^h_n)\right]}{\Delta t_n}\right)_\Omega-\left(\nabla w^h_5,\left(\rho^h_{n+\frac{1}{2}}V^h_{n+\frac{1}{2}}\theta^h_{n+\frac{1}{2}}\right.\right.\\
&\left.\left.-\theta^h_{n+\frac{1}{2}}H^h_{n+\frac{1}{2}}+\frac{|\nabla\rho^h_{n+\frac{1}{2}}|^2}{2\mathrm{We}}+\frac{\rho^h_{n+\frac{1}{2}}\theta^h_{n+\frac{1}{2}}}{\mathrm{We}}\nabla\cdot\left(\frac{\nabla\rho^h_{n+\frac{1}{2}}}{\theta^h_{n+\frac{1}{2}}}\right)+\rho^h_{n+\frac{1}{2}}|\mathbf{u}^h_{n+\frac{1}{2}}|^2\right)\mathbf{u}^h_{n+\frac{1}{2}}\right)_\Omega\\
&+\left(\nabla w^h_5,\boldsymbol{\tau}^h_{n+\frac{1}{2}}\mathbf{u}^h_{n+\frac{1}{2}}\right)_\Omega+\left(\nabla w^h_5,\boldsymbol{\varsigma}^h_{n+\frac{1}{2}}\mathbf{u}^h_{n+\frac{1}{2}}\right)_\Omega-\left(\nabla w^h_5,\mathbf{q}^h_{n+\frac{1}{2}}+\boldsymbol{\Pi}^h_{n+\frac{1}{2}}\right)_\Omega\\
&-\left(w^h_5,\rho^h_{n+\frac{1}{2}}\mathbf{b}\cdot\mathbf{u}^h_{n+\frac{1}{2}}\right)_\Omega-\left(w^h_5,\rho^h_{n+\frac{1}{2}}r\right)_\Omega=0,
\end{aligned} \tag{11}
$$

$$
\begin{aligned}
\mathbf{B}^A(w^h_6;\mathbf{Y}^h_{n+1}):=&\left(w^h_6,V^h_{n+\frac{1}{2}}-\frac{1}{2\theta^h_{n+\frac{1}{2}}}\left(\left(\nu_{loc}(\rho^h_n,\theta^h_{n+\frac{1}{2}})+\nu_{loc}(\rho^h_{n+1},\theta^h_{n+\frac{1}{2}})\right)\right.\right.\\
&\left.\left.+\frac{[\![\rho^h_n]\!]^2}{12}\frac{\partial^2\nu_{loc}}{\partial\rho^2}(\rho^h_n,\theta^h_{n+\frac{1}{2}})\right)-\frac{\mathbf{u}^h_n\cdot\mathbf{u}^h_{n+1}}{2\theta^h_{n+\frac{1}{2}}}\right)_\Omega-\left(\nabla w^h_6,\frac{\nabla\rho^h_{n+\frac{1}{2}}}{\mathrm{We}\theta^h_{n+\frac{1}{2}}}\right)_\Omega=0.
\end{aligned} \tag{12}
$$

In our work, Non-Uniform Rational B-Splines (NURBS) basis functions are used to define $\mathscr{V}^h$ as well as the computational domain. Consequently, this approach may

be considered as isogeometric analysis method [7]. The main results of the fully discrete scheme (9)-(12) are stated in the following two theorems.

Theorem 1. *The solutions of the fully discrete scheme (9)-(12) satisfy*

$$\int_\Omega \left(\frac{H(\rho^h_{n+1},\theta^h_{n+1}) - H(\rho^h_n,\theta^h_n)}{\Delta t_n} + \nabla\cdot\left(H(\rho^h_{n+\frac{1}{2}},\theta^h_{n+\frac{1}{2}})\mathbf{u}^h_{n+\frac{1}{2}}\right) - \nabla\cdot\left(\frac{\mathbf{q}^h_{n+\frac{1}{2}}}{\theta^h_{n+\frac{1}{2}}}\right) + \frac{\rho^h_{n+\frac{1}{2}} r}{\theta^h_{n+\frac{1}{2}}}\right) dV_{\mathbf{x}} = -\int_\Omega \frac{1}{\theta^h_{n+\frac{1}{2}}}\boldsymbol{\tau}^h_{n+\frac{1}{2}} : \nabla\mathbf{u}^h_{n+\frac{1}{2}} dV_{\mathbf{x}} - \int_\Omega \frac{\kappa|\nabla\theta^h_{n+\frac{1}{2}}|^2}{\left(\theta^h_{n+\frac{1}{2}}\right)^2} dV_{\mathbf{x}}$$

$$-\int_\Omega \frac{1}{\theta^h_{n+\frac{1}{2}}\Delta t_n}\left(\frac{[\![\rho^h_n]\!]^4}{24}\frac{\partial^3 \nu_{loc}}{\partial\rho^3}(\rho^h_{n+\xi_1},\theta^h_{n+\frac{1}{2}}) - \frac{[\![\theta^h_n]\!]^4}{24}\frac{\partial^3 H}{\partial\theta^3}(\rho^h_{n+\frac{1}{2}},\theta^h_{n+\xi_2})\right) dV_{\mathbf{x}} \le 0.$$

Theorem 2. *The local truncation error in time* $\boldsymbol{\Theta}(t) = \left(\Theta_\rho(t);\boldsymbol{\Theta}^T_{\mathbf{u}}(t);\Theta_E(t)\right)^T$ *can be bounded by* $|\boldsymbol{\Theta}(t_n)| \le K\Delta t_n^2 \mathbf{1}_5$ *for all* $t_n \in [0,T]$*, where* K *is a constant independent of* Δt_n *and* $\mathbf{1}_5 = (1;1;1;1;1)^T$.

The proofs of the above two theorems can be found in [10]. Theorem 1 states that the method is unconditionally entropy stable, because $\partial^3\nu_{loc}/\partial\rho^3 \ge 0$ and $\partial^3 H/\partial\theta^3 \le 0$, which follow from properties of the van der Waals fluid. Theorem 2 establishes the second-order time-accuracy of the method.

4 Boiling

To obtain successful boiling simulations, there are several additional modeling considerations. First, the transport parameters need to be density dependent in order to differentiate the properties of the liquid and vapor phases. In our simulations, the dimensionless viscosity coefficient and the dimensionless conductivity are modeled as

$$\bar{\mu} = C^{boil}_\mu \rho, \qquad \kappa = C^{boil}_\kappa \rho,$$

with C^{boil}_μ and C^{boil}_κ being constants independent of ρ. Second, the gravity effect need to be taken into account to generate buoyancy. The dimensionless body force $\mathbf{b}$ is chosen as $\mathbf{b} = (0;0;-0.025)^T$ for the three-dimensional case and $\mathbf{b} = (0;-0.025)^T$ for the two-dimensional case. Third, the ninety-degree contact angle boundary condition is used for the density variable, and the slip boundary condition is applied to the velocity. To specify the boundary condition for $Y_5 = -1/\theta$, the boundary $\partial\Omega$ is divided into three non-overlapping parts:

$$\partial\Omega = \Gamma_i \cup \Gamma_b \cup \Gamma_v, \qquad \Gamma_i = \{\mathbf{x}\in\partial\Omega \,|\, \mathbf{n}(\mathbf{x})\cdot\mathbf{b} < 0\},$$

$$\Gamma_b = \{\mathbf{x} \in \partial\Omega | \mathbf{n}(\mathbf{x}) \cdot \mathbf{b} > 0\}, \quad \Gamma_v = \{\mathbf{x} \in \partial\Omega | \mathbf{n}(\mathbf{x}) \cdot \mathbf{b} = 0\}.$$

With the above partition, the boundary condition for Y_5 is

$$\begin{aligned} Y_5 &= -\frac{1}{0.950} + \delta_{Y_{5,h}}(\mathbf{x}), \quad \text{on } \Gamma_b \times (0,T), \\ Y_5 &= -\frac{1}{0.775} + \delta_{Y_{5,c}}(\mathbf{x}), \quad \text{on } \Gamma_t \times (0,T), \\ -\mathbf{q} \cdot \mathbf{n} &= 0, \qquad\qquad\qquad\quad \text{on } \Gamma_v \times (0,T), \end{aligned}$$

wherein $\delta_{Y_{5,h}}(\mathbf{x})$ and $\delta_{Y_{5,c}}(\mathbf{x})$ are small scalar perturbation functions that mimic the uneven temperature distribution on the solid surface. The initial conditions represent a static free surface, with liquid in the bottom region and vapor in the top region. It is worth emphasizing that, in contrast to existing boiling models, there is no artificial manipulation used to serve as boiling onset in this model; the initial liquid and vapor densities are uniform with no perturbations.

4.1 Two-dimensional nucleate boiling

In this example, we simulate boiling flows in a two-dimensional rectangular domain $\Omega = (0,1) \times (0,0.5)$. The material parameters are chosen as $\mathrm{We} = 8.401 \times 10^6$, $\gamma = 1.333$, $C_\mu^{boil} = 1.150 \times 10^{-4}$, and $C_\kappa^{boil} = 1.725 \times 10^{-5}$. The initial conditions for this problem are

$$\begin{aligned} \rho_0(\mathbf{x}) &= 0.3660 - 0.2971 \tanh\left(\frac{x_2 - 0.35}{2}\sqrt{\mathrm{We}}\right), \\ \mathbf{u}_0(\mathbf{x}) &= \mathbf{0}, \\ \theta_0(\mathbf{x}) &= 0.775. \end{aligned}$$

The perturbation for the temperature on the boundary $\delta_{Y_{5,h}}(\mathbf{x})$ and $\delta_{Y_{5,c}}(\mathbf{x})$ are uniform random distributions and satisfy

$$\delta_{Y_{5,h}}(\mathbf{x}) \in [-5.0 \times 10^{-2}, 5.0 \times 10^{-2}], \quad \delta_{Y_{5,c}}(\mathbf{x}) \in [-5.0 \times 10^{-3}, 5.0 \times 10^{-3}].$$

The spatial mesh consists of 2048×1024 quadratic NURBS elements. The problem is integrated up to the final time $T = 100.0$ with time step fixed as $\Delta t = 5.0 \times 10^{-4}$. In Figure 1, snapshots of the density are depicted at different time steps. It can be observed that tiny vapor bubbles are generated at discrete sites of the heated wall surface during the initial times. The increase of bubble size leads to the increase of buoyancy. At about $t = 18.75$, the first three bubbles get detached from the bottom. More bubbles are generated on the bottom surface subsequently. Interestingly, small droplets can be observed at $t = 62.5$ and $t = 100.0$ as a result of the breakage of the liquid film when the vapor bubbles reach the free surface. There are 30 bubbles formed in the time interval of $0 < t < 100$.

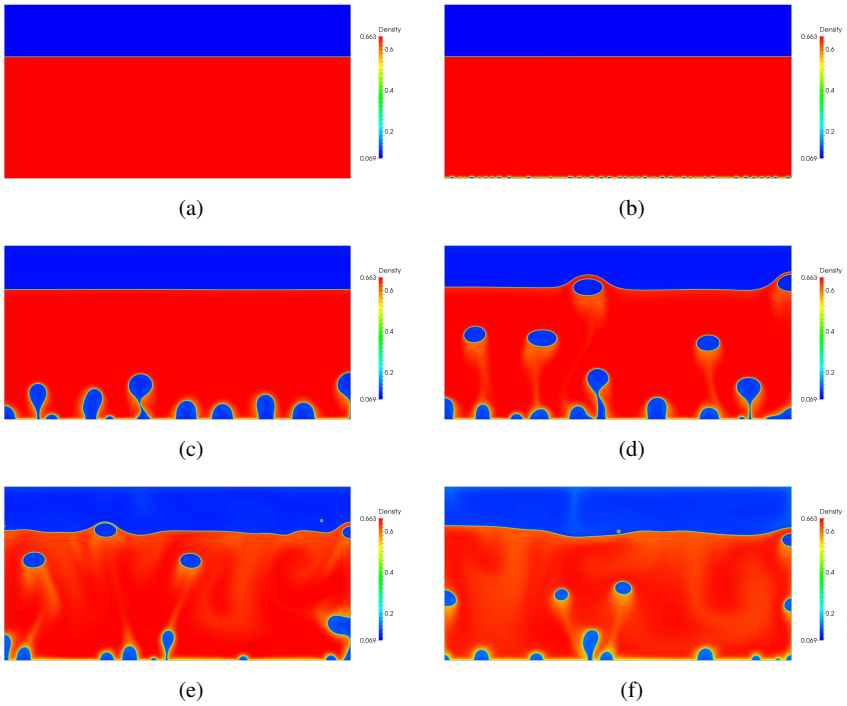

Fig. 1 Two-dimensional nucleate boiling simulation: Density profiles at (a) $t = 0.0$, (b) $t = 1.25$, (c) $t = 18.75$, (d) $t = 31.25$, (e) $t = 62.5$, and (f) $t = 100.0$.

4.2 Two-dimensional film boiling

In the second example, the same two-dimensional problem considered in the preceding section is simulated again with a different parameter C_μ^{boil}. Here, the parameter C_μ^{boil} is chosen to be 4.600×10^{-4}, which is four times larger than that of the previous example. Since the fluid motion in this example is slower, the simulation is integrated in time up to $T = 500.0$. All the other conditions are identical to those of the previous case. In Figure 2, snapshots of the density at different time steps are depicted. A thin vapor film is gradually generated at the bottom during the early stage of the simulation. As time evolves, the interface becomes unstable and there are vapor bubbles formed. From $t = 200.0$ to $t = 225.0$, the first two vapor bubbles pinch off from the vapor film and rise upward in ellipsoidal shapes. This process repeats itself periodically. By final time $t = 500.0$, there are seven bubbles detached from the vapor film.

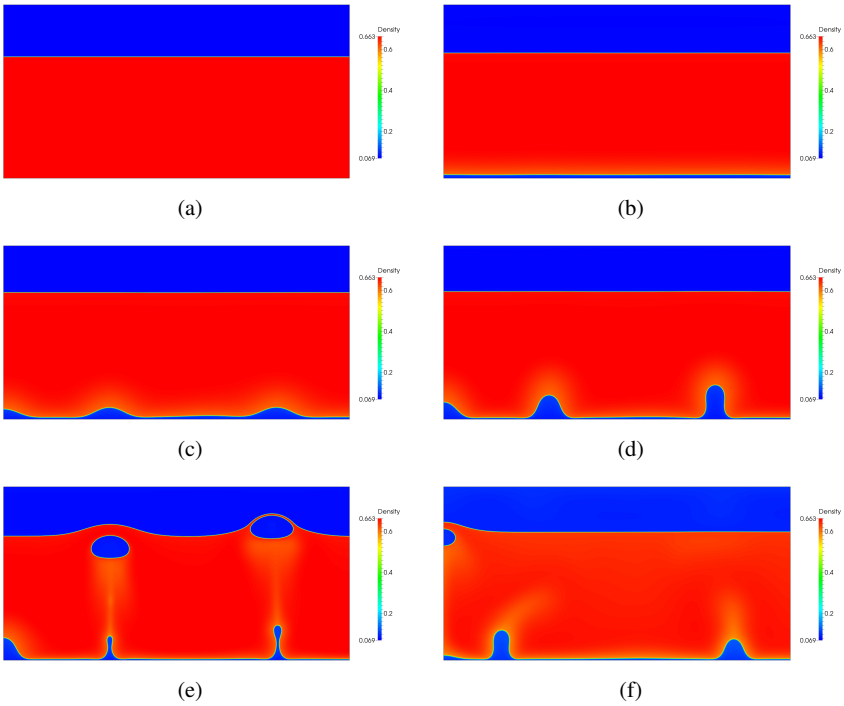

Fig. 2 Two-dimensional film boiling simulation: Density profiles at (a) $t = 0.0$, (b) $t = 100.0$, (c) $t = 175.0$, (d) $t = 200.0$, (e) $t = 225.0$, and (f) $t = 500.0$. The generation of the thin vapor film is visible at $t = 100.0$.

4.3 Three-dimensional boiling

As the last example, we simulate the Navier-Stokes-Korteweg equations in a three-dimensional domain $\Omega = (0,1) \times (0,0.5) \times (0,0.25)$. The material properties are chosen as $\mathrm{We} = 6.533 \times 10^5$, $\gamma = 1.333$, $C_\mu^{boil} = 1.289 \times 10^{-4}$, and $C_\kappa^{boil} = 7.732 \times 10^{-5}$. The initial conditions for this three-dimensional problem are

$$\begin{aligned}
\rho_0(\mathbf{x}) &= 0.33565 - 0.26675 \tanh\left(\frac{x_3 - 0.15}{2}\sqrt{\mathrm{We}}\right), \\
\mathbf{u}_0(\mathbf{x}) &= \mathbf{0}, \\
Y_{5,0}(\mathbf{x}) &= -1.2334 - 0.0569 \tanh\left(\frac{x_3 - 0.15}{2}\sqrt{\mathrm{We}}\right).
\end{aligned}$$

The perturbations of the temperature on the boundary $\delta_{Y_{5,h}}(\mathbf{x})$ and $\delta_{Y_{5,c}}(\mathbf{x})$ are uniform random distributions and satisfy

$$\delta_{Y_{5,h}}(\mathbf{x}) \in [-5.0 \times 10^{-2}, 5.0 \times 10^{-2}], \quad \delta_{Y_{5,c}}(\mathbf{x}) \in [-5.0 \times 10^{-3}, 5.0 \times 10^{-3}].$$

The spatial mesh consists of $600 \times 300 \times 150$ quadratic NURBS elements. The problem is integrated in time up to $T = 20.0$ with a fixed time step size $\Delta t = 2.0 \times 10^{-3}$. In Figure 3, snapshots of density isosurfaces and velocity streamlines are presented. At the initial stage, there is an unstable vapor film formed over the heated wall surface. This film soon separates into isolated vapor bubbles located at random sites. Since the simulation domain is very shallow in the vertical direction, these bubbles reach the free surface before they get fully detached from the bottom. When these high-temperature vapor bubbles reach the cooled top surface, they condense into liquid droplets instantaneously (see Fig. 3 (e)). At $t = 20.0$, a second round of vapor bubbles is clearly generated on the bottom and the liquid droplets on the top surface merge together.

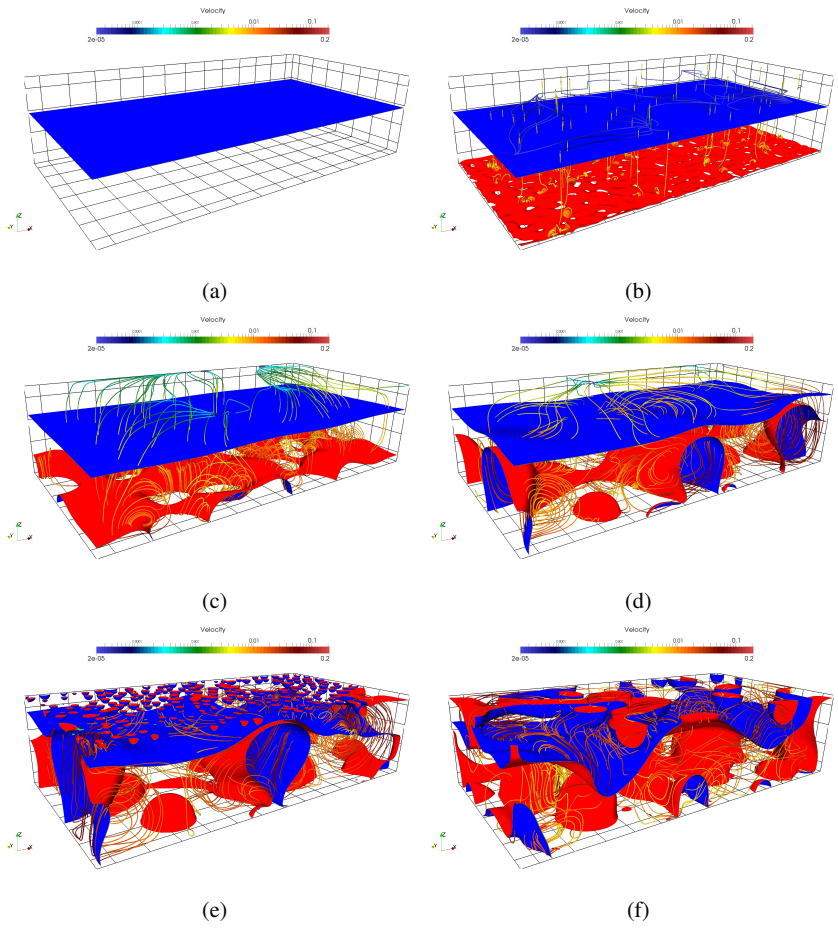

Fig. 3 Three-dimensional boiling simulation: Density isosurfaces and velocity streamlines at (a) $t = 0.0$, (b) $t = 0.6$, (c) $t = 5.0$, (d) $t = 11.0$, (e) $t = 14.0$, and (f) $t = 20.0$.

5 Conclusion

In this work, we presented theoretical and numerical methodologies for the study of boiling, capable of describing complicated phase transition phenomena without resorting to empirical assumptions. Our algorithm is provably entropy-stable and second-order accurate in time. It provides a unified predictive framework for nucleate and film boiling in two and three dimensions. In the future, the presented methodologies will be applied to the study of other important phase transition phenomena, such as cavitation, spray and mist formation.

Acknowledgements This work was partially supported by the Office of Naval Research under contract number N00014-08-1-0992.

References

1. Anderson, D.M., McFadden, G.B., Wheeler, A.A.: Diffuse-interface methods in fluid mechanics. Annual Review of Fluid Mechanics **30**, 139-165 (1998)
2. Dhir, V.K.: Boiling heat transfer. Annual Review of Fluid Mechanics **30**, 365–401 (1998)
3. Dunn, J.E., Serrin, J.: On the thermomechanics of interstitial working. Archive for Rational Mechanics and Analysis **88**, 95-133 (1985)
4. Gomez, H., Hughes, T.J.R., Nogueira, X., Calo, V.: Isogeometric analysis of the Navier-Stokes-Korteweg equations. Computer Methods in Applied Mechanics and Engineering **199**, 1828-1840 (2010)
5. Gomez, H., Hughes, T.J.R.: Provably unconditionally stable, second-order time-accurate, mixed variational methods for phase-field models. Journal of Computational Physics **230**, 5310-5327 (2011)
6. Hughes, T.J.R., Franca, L.P., Mallet, M.: A new finite element formulation for computational fluid dynamics: I. Symmetric forms of the compressible Euler and Navier-Stokes equations and the second law of thermodynamics. Computer Methods in Applied Mechanics and Engineering **54**, 223-234 (1986)
7. Hughes, T.J.R., Cottrell, J.A., Bazilevs, Y.: Isogeometric analysis: CAD, finite elements, NURBS, exact geometry and mesh refinement. Computer Methods in Applied Mechanics and Engineering **194**, 4135-4195 (2005)
8. Juric, D., Tryggvason, G.: Computation of boiling flows. International Journal of Multiphase Flow **24**, 387–410 (1998)
9. Liu, J., Gomez, H., Evans, J.A., Landis, C.M., Hughes, T.J.R.: Functional Entropy Variables: A New Methodology for Deriving Thermodynamically Consistent Algorithms for Complex Fluids, with Particular Reference to the Isothermal Navier-Stokes-Korteweg Equations. Journal of Computational Physics **248**, 47-86, (2013)
10. Liu, J., Landis, C.M., Gomez, H., Hughes, T.J.R.: Liquid-Vapor Phase Transition: Thermomechanical Theory, Entropy Stable Numerical Formulation, and Boiling Simulations, Computer Methods in Applied Mechanics and Engineering, submitted.
11. Shakib, F., Hughes, T.J.R., Johan, Z.: A new finite element formulation for computational fluid dynamics: X. The compressible Euler and Navier-Stokes equations. Computer Methods in Applied Mechanics and Engineering **89**, 141-219 (1991)